Defect production in Si(100) by ^{19}F, ^{28}Si, ^{40}Ar, and ^{131}Xe implantation at room temperature

G. Bai and M-A. Nicolet
California Institute of Technology, Pasadena, California 91125

(Received 13 May 1991; accepted for publication 1 July 1991)

We used x-ray double-crystal diffractometry and MeV ^4He channeling spectrometry to study quantitatively the damage produced in Si(100) at room temperature by 230-keV ^{19}F, 230-keV ^{28}Si, 250-keV ^{40}Ar, or 570-keV ^{131}Xe implantation. The measured defect concentration and the perpendicular strain have the same depth profile, and both are depleted near the surface compared to the Frenkel pair concentration calculated from computer simulation. The perpendicular strain is proportional to the defect concentration with a coefficient of $B \sim 0.01$ common to all implanted species. The maximum value of the perpendicular strain and of the defect concentration rises nonlinearly with the dose for all species. The damage produced by different implanted species depends on the dose in approximately the same way save for a scaling factor of the dose. In the regime of low damage, the strain and the defect concentration rise linearly with increasing dose. The slope of this rise with dose increases with the square of the Frenkel pairs produced per unit dose of incident ions, as calculated from computer simulations. This fact means that stable defects produced by room-temperature implantation in Si(100) cannot be predicted by a linear cascade model.

I. INTRODUCTION

Ion implantation is routinely used in the fabrication of Si-based integrated circuits. Details of the associated defects production and their stability are still poorly understood despite extensive research in the last two decades.[1–11] In recent years, ion implantation technology has found new applications in areas such as ion-beam-induced epitaxial growth[12] and synthesis of buried heterostructures.[13] The critical role of point defects produced by ion implantation in enhanced diffusion of dopants upon thermal annealing has also been recognized.[14] An improved understanding of ion-induced defect production and annealing promises deepened insights in these phenomena.

In a previous paper, we employed both x-ray double-crystal diffractometry and MeV ^4He channeling spectrometry to analyze quantitatively the damage produced by self-implantation in Si(100) at room temperature.[15] We extend here the investigation of the production of defects and their stability in room-temperature implanted Si(100) to ions of vastly different atomic numbers and masses. Some perspectives on the nature of defects produced by the implantation and their stability are discussed in the light of the experimental results.

II. EXPERIMENTAL PROCEDURES

Ions of either 230-keV ^{19}F, 230-keV ^{28}Si, 250-keV ^{40}Ar, or 570-keV ^{13}Xe were implanted into Si(100) at room temperature in high vacuum ($\sim 10^{-7}$ Torr). The beam flux was limited to $\leqslant 0.5\ \mu A/cm^2$ to minimize the sample heating. The ranges of implanted ions in Si(100), calculated from TRIM 88 simulation,[16] vary from $\sim 0.2\ \mu m$ for 570-keV ^{131}Xe to $\sim 0.4\ \mu m$ for 230-keV ^{19}F. The doses were chosen to produce a spectrum that covers the entire range of damage, from a lightly damaged crystal to one with a buried continuous amorphous layer.

2-MeV ^4He channeling measurements were used to extract the defect concentration in the implanted layer. The strain induced by the damage was obtained by fitting the measured x-ray rocking curves to ones calculated from the dynamical diffraction model.[17]

III. RESULTS OF 230-keV ^{19}F IMPLANTATION

Channeling spectra of 230-keV ^{19}F-implanted Si(100) samples are shown in Fig. 1. Implantation to a dose of $5 \times 10^{14}/cm^2$ (curve a in Fig. 1) produces only a marginally detectable dechanneling yield above the background yield of a virgin sample (labeled as virgin in Fig. 1), while implantation to a dose of $2 \times 10^{15}/cm^2$ (curve d in Fig. 1) produces a region in the channeling spectrum where the channeling yield equals the random one. We shall refer to the corresponding region in the sample as a continuous amorphous layer for the rest of this paper.

The depth profile of defect concentration, $c_D(x)$, is extracted from the channeling spectrum according to the equation[15]

$$\gamma_D(x) = c_D(x) + P_D(x)[1 - c_D(x)], \tag{1}$$

where x is the depth from the surface. The dechanneling factor, $\gamma_D(x)$, is directly obtained from the channeling yields normalized to the random yields of the damaged sample, $\chi_D(x)$, and of the virgin sample, $\chi_V(x)$,

$$\gamma_D(x) \equiv \frac{\chi_D(x) - \chi_V(x)}{1 - \chi_V(x)} \in [0,1]. \tag{2}$$

The dechanneling probability, $P_D(x)$, in the single scattering approximation, is

 0021-8979/91/073551-05$03.00

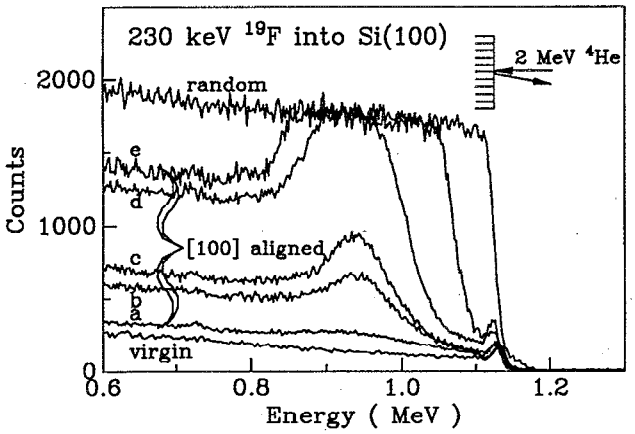

FIG. 1. Backscattering spectra of 2-MeV $^4He^+$ incident along a near-normal random and [100] aligned directions for a virgin Si(100) sample and for samples implanted at room temperature with 230-keV ^{19}F to doses of (a) 5, (b) 9, (c) 10, (d) 20, and (e) 50×10^{14}/cm^2. The scattering angle of the detected ^{4}He is 170°.

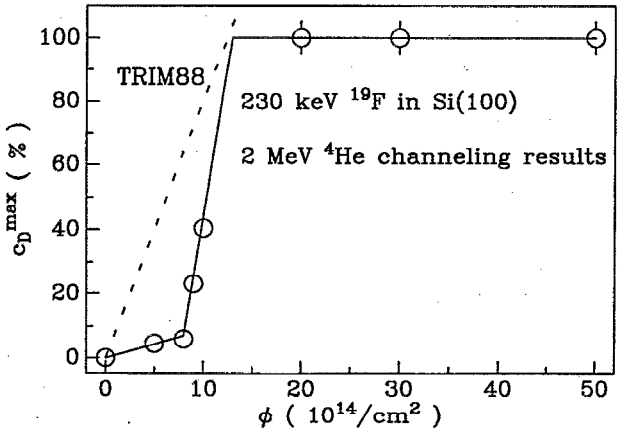

FIG. 3. Maximum defect concentration extracted from the channeling spectra of Fig. 1, and of additional ones, as a function of the ^{19}F dose. The solid line highlights the trend. The dashed line is the maximum value in the depth profile of the Frenkel pair concentration predicted by the TRIM 88 simulation of 230-keV ^{19}F implanted into an amorphous Si target.

$$P_D(x)=n\sigma_D\int_0^x c_D(x')dx', \tag{3}$$

where n is the atomic density of the target and σ_D is the dechanneling cross section of individual pointlike defect. We solve Eqs. (1) and (3) numerically from the input data $\gamma_D(x)$, and obtain $c_D(x)$. Figure 2 illustrates the solution for the sample implanted to 10^{15}/cm^2 (c in Fig. 1). $P_D(x)$ is obtained by adjusting the fitting parameter σ_D so that the boundary condition that P_D equals γ_D beyond the damaged region is satisfied. The value of σ_D for this fit is $(5.6\pm0.5)\times10^{-19}$ cm^2. The dotted line is the depth profile of defect concentration $c_D(x)$. We found that c_D is not sensitive to the choice of σ_D. c_D has similar depth dependence as that obtained for the self-implanted Si(100).[15] In particular, the defect concentration near the surface is again depleted compared to that predicted from TRIM 88 simulation. This fact suggests that the surface is an effective sink for the defects.

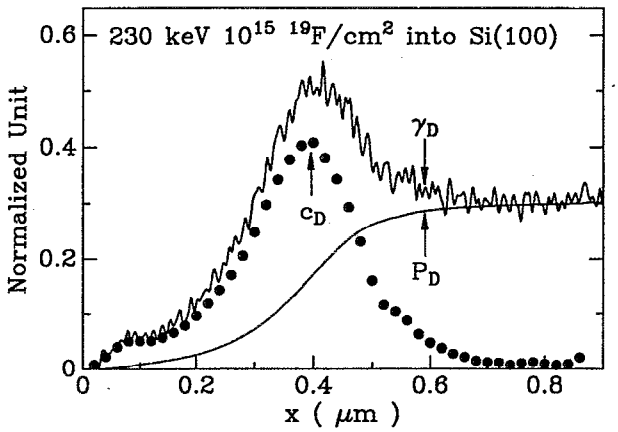

FIG. 2. Dechanneling factor γ_D calculated from the normalized yields of the virgin and implanted samples (virgin and c in Fig. 1) is plotted as a function of the depth x from the sample surface. The dechanneling probability P_D that satisfies the boundary condition that P_D equals γ_D beyond the damaged region, and the extracted defect concentration c_D(●) are also shown.

The same procedure was applied to the samples with other ^{19}F doses, and the defect concentration $c_D(x)$ was extracted. The fitting parameter σ_D decreases linearly as the damage c_D increases. The value of σ_D is $(8\pm1)\times10^{-19}$ cm^2 for the sample implanted to 5×10^{14}/cm^2, and becomes $(2.6\pm0.1)\times10^{-19}$ cm^2 for the one implanted to 5×10^{15}/cm^2. $c_D(x)$ peaks at ~0.4 μm for all doses and has a similar shape to that shown in Fig. 2 (●).

The maximum value of the defect concentration profile is plotted as a function of the ^{19}F dose in Fig. 3. The dose dependence is highly nonlinear and similar to that observed for the self-implanted Si(100). The damage here can also be categorized into three regimes, I, II, III, corresponding to low damage, enhanced damage production, and the formation of a continuous amorphous layer, respectively (see Ref. 15 for a detailed discussion). In particular, we notice that the transition from I to II occurs at a defect concentration of $\sim10\%$, the same damage level as that found in the self-implanted samples. This similarity suggests that the general character of damage production in Si(100) by room-temperature implantation is insensitive to the implanted species. The critical dose ϕ_{cr}($\sim 8\times10^{14}$/cm^2) of the ^{19}F-implanted sample, however, is more than twice of that for ^{28}Si implantation ($\sim3\times10^{14}$/cm^2). This is partly due to the fact that each ^{19}F ion produces less Frenkel pairs than each ^{28}Si ion does. The dose required to produce the same amount of Frenkel pairs is hence greater for ^{19}F than for ^{28}Si. Figure 3 also shows the maximum of the Frenkel pairs concentration versus the implantation dose, calculated from TRIM 88 simulation (dashed line). A displacement energy of 15 eV (Ref. 6) and a binding energy of 1 eV were chosen as the input parameters. The concentration of the measured defects is much less than that of the Frenkel pairs at the low

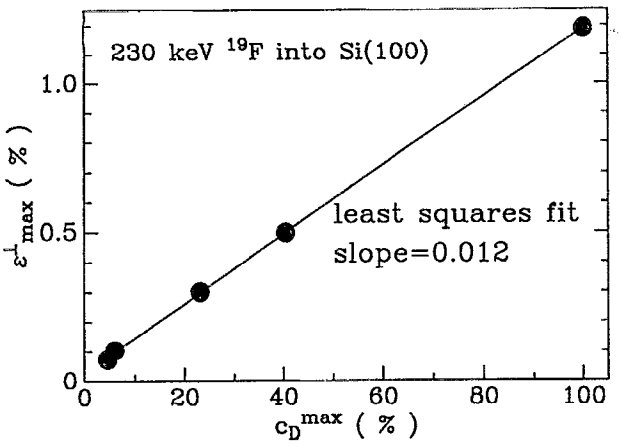

FIG. 4. Relationship between the maximum values of the perpendicular strain from x-ray diffraction measurements and the defect concentration from 2-MeV ^{4}He channeling measurements. The solid line is the least-squares fit of a linear function to the data (●).

damage level (regime I). The initial slope of the measured defect concentration versus dose is only ~0.2 times that of the Frenkel pairs. This demonstrates that the majority of the initially produced defects are mobile at room temperature and recombine.[18]

X-ray rocking curves for both symmetrical (400) and asymmetrical (311) diffractions of the implanted samples were taken and analyzed with the dynamical diffraction model. The parallel strain is zero for all the samples, meaning that the lateral spacing of the damaged layer is confined to be the same as that of the unimplanted substrate. The perpendicular strain is always positive and has the same depth dependence as the defect profile (● in Fig. 2). The maximum value in the perpendicular strain profile rises nonlinearly with the ^{19}F dose. It has the same dose dependence as that of the defect concentration of Fig. 3, with the same critical dose ϕ_{cr}, $\sim 8 \times 10^{14}/cm^2$ (see Fig. 5). The transition from regime I to II occurs at a strain value of ~0.15%. All these results are similar to those obtained for the self-implanted Si(100).[15]

Furthermore, we discover that, as for the ^{28}Si-implanted samples, the strain in the damaged layer of the ^{28}F-implanted samples is also proportional to the defect concentration over the whole range of strain and damage (Fig. 4),

$$\epsilon^{\perp} = Bc_D. \tag{4}$$

The coefficient B equals 0.012, which is also the same as for self-implanted Si(100) (B=0.013).[15] This relationship between the defects and the induced strain is thus insensitive to the implanted species, but an intrinsic property of the Si target.

IV. GENERALIZATION TO ANY IONS

X-ray rocking curve analyses of 250-keV ^{49}Ar- and 570-keV ^{131}Xe-implanted samples were also performed. The parallel strain is again zero. The perpendicular strain is positive and its depth profiles all have the similar shape as that shown Fig. 2 (●). In particular, the strain near the surface is always depleted in comparison with that predicted by TRIM 88. The maximum perpendicular strain as a function of dose is plotted in Fig. 5 for all ions. Firstly, they all show similarly nonlinear dose dependencies. The nonlinearity is strongest for ^{19}F and ^{28}Si, and weakest for ^{131}Xe. Secondly, the transition from regime I to II occurs at about the same strain value of ~0.1%–0.2%, independent of the ion species, while the critical dose decreases from $\sim 8 \times 10^{14}/cm^2$ for the light ^{19}F to $\sim 10^{13}/cm^2$ for the heavy ^{131}Xe. The key difference of the samples implanted with different ions is the different scale of the dose (see Fig. 5). We therefore choose the dose, ϕ_{mid}, when $\epsilon^{\perp}_{max}$ is at the middle value of ~0.6% in Fig. 5, as a natural unit for each ion species, and replot the maximum perpendicular strain as a function of the normalized dose (Fig. 6). One sees that as a function of this normalized dose, $\epsilon^{\perp}_{max}$ follows an approximately universal curve (solid line in Fig. 6). This fact means that the damage effect of different implantation species is approximately equivalent up to a scaling of the implantation dose. One systematic small deviation from the universal function is that the slope in regime II for light ions (^{19}F, ^{28}Si) is larger than that for heavy ions (^{40}Ar, ^{131}Xe). In other words, the nonlinearity for light ions is more pronounced than that for heavy ions. This tendency is in accord with our previous proposition that the nonlinearity arises from the recombination of simple vacancy-interstitial defects at room temperature.[15]

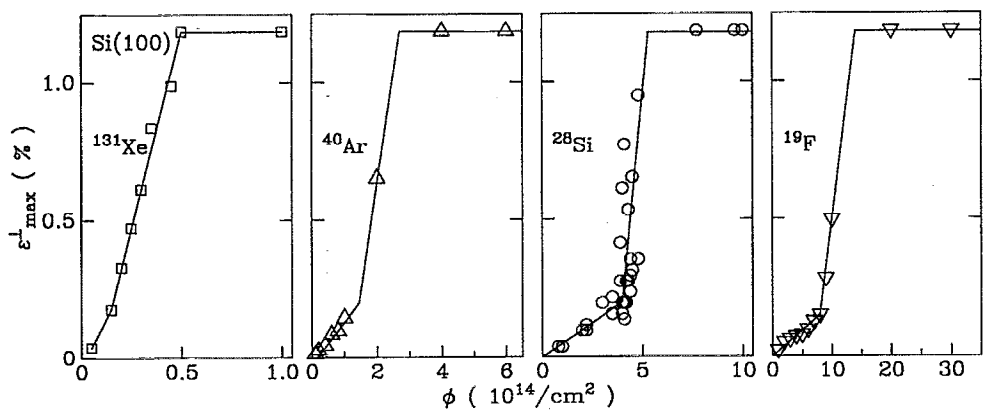

FIG. 5. Maximum perpendicular strain obtained by fitting the dynamical x-ray diffraction simulations to the experimental rocking curves as a function of the implantation dose for four different ions. The solid line stresses the trend.

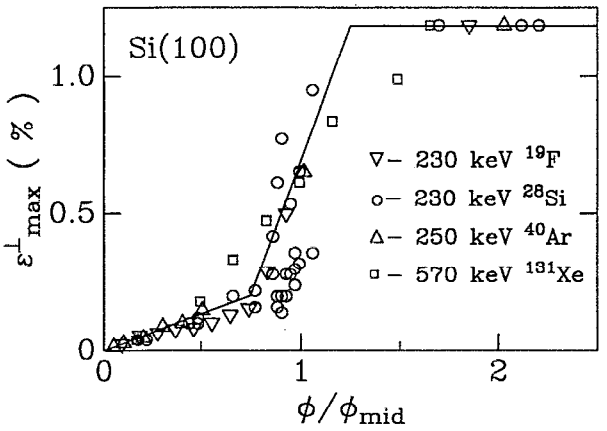

FIG. 6. Maximum perpendicular strain for four implantation species is plotted as a function of the normalized dose. The normalization parameter ϕ_{mid} is chosen for each ion as the dose where $\epsilon^{\perp}_{max}$, is at the middle value of ~0.6% in Fig. 5. The solid line stresses the trend.

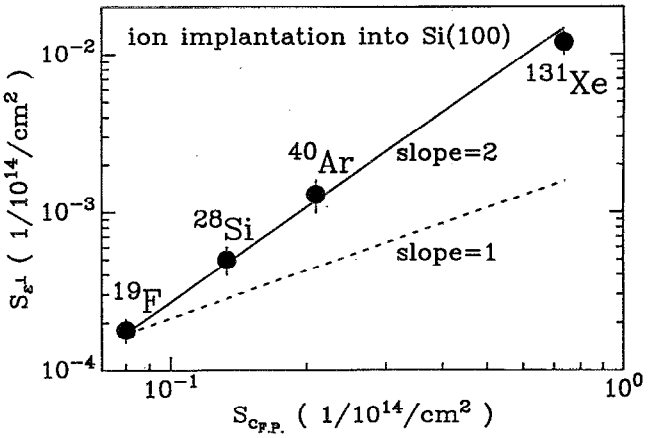

FIG. 7. Initial (regime I) slope of the maximum perpendicular strain vs the dose as a function of the Frenkel pair concentration per unit dose for various incident ions.

Light ions produce defects which are sparsely distributed within a large cascade volume and consist mainly of isolated interstitials and vacancies so that few stable complexes are formed and most defects recombine. On the other hand, heavy ions produce defects which distribute densely in a small cascade volume so that the formation of defect complexes and clusters which are stable at room temperature is enhanced.

Based on the results on the linear relationship between the strain and the defect concentration obtained in samples implanted with ^{19}F and ^{28}Si (Fig. 4 and Ref. 15), we assume that this same linear relationship ($\epsilon^{\perp} \doteq 0.01 c_D$) also applies to other ions. The common critical perpendicular strain $\epsilon^{\perp}_{cr}$(~ 0.1%–0.2%) of Figs. 5 and 6 for various ions thus means that the critical defect concentration c^{cr}_D is also the same (~10%–20%) for all ions. Above this damage level, the defected crystal becomes unstable and the damage rises rapidly (regime II) until a continuous amorphous layer forms (regime III) (see Fig. 3).

In the lightly damaged regime I, the strain (and hence defect concentration) increases approximately linearly with dose,

$$\epsilon^{\perp}_{max} = S_{\epsilon^{\perp}} \phi, \tag{5}$$

where $S_{\epsilon^{\perp}}$ is the slope of $\epsilon^{\perp}_{max}$ vs ϕ. The slope $S_{\epsilon^{\perp}}$ increases from ~0.02%/(10^{14}/cm^2) for ^{19}F to ~1.2%/(10^{14}/cm^2) for ^{131}Xe.

To put these values into perspective, we computed the maximum of the Frenkel pair concentration per unit dose of incident ions, $S_{c_{FP}}$, by TRIM 88. $S_{c_{FP}}$ measures the amount of displacement produced by each incident ion. For a given implantation dose ϕ, the maximum Frenkel concentration c^{max}_{FP} equals $S_{c_{FP}}$ times the dose ϕ. The heavier an incident ion is, the more damage it produces, and hence the larger $S_{c_{FP}}$ becomes. $S_{c_{FP}}$ increases from ~8%/(10^{14}/cm^2) for ^{19}F to ~74%/(10^{14}/cm^2) for ^{131}Xe.

Figure 7 shows the measured slope $S_{\epsilon^{\perp}}$ as a function of the calculated $S_{c_{FP}}$ from TRIM 88 for four ions (●). The solid line represents a quadratic dependence of the slope on $S_{c_{FP}}$ and the dashed line a linear dependence. It is evident from the figure that the slope $S_{\epsilon^{\perp}}$ has an approximate quadratic dependence on $S_{c_{FP}}$,

$$S_{\epsilon^{\perp}} \propto S^2_{c_{FP}}. \tag{6}$$

We also plot the critical dose ϕ_{cr} as a function of $S_{c_{FP}}$ for the four ions, and discover that

$$\phi_{cr} \propto S^{-2}_{c_{FP}}. \tag{7}$$

Combining these results, we find that the critical strain defined by

$$\epsilon^{\perp}_{cr} \equiv S_{\epsilon^{\perp}} \phi_{cr} \tag{8}$$

is a constant, 0.17%, independent of incident ions. This result agrees with that obtained previously from Fig. 5.

The defect concentration c_D is proportional to the strain $\epsilon^{\perp}$ in room-temperature-implanted Si(100). One therefore has the following relationship, according to Eq. (6):

$$S_{c_D} \propto S^2_{c_{FP}}, \tag{9}$$

where S_{c_D} is the slope of the defect concentration from the channeling analysis of the implanted samples in regime I versus dose. It states that the stable defect concentration rises quadratically as the Frenkel pair concentration per unit ion dose increases. This fact means that the stable defects produced by room-temperature implantation in Si(100) cannot be predicted by the linear cascade model. It supports our previous hypothesis that the simple vacancy-interstitial defects are not stable at room temperature. They recombine or form defect complex and clusters, and it is these that are stable at room temperature. The fraction of the various microstructural defects depends on the density of the Frenkel pairs initially produced by an incident ion in a cascade volume. A low density in a large volume (for light ion) results in a large fraction of simple defects, while a high density in a small volume (for heavy ion)

results in a large fraction of defect complex and clusters. This explains qualitatively the nonlinear dependence of S_{c_D} on $S_{c_{FP}}$.

V. CONCLUSION

Implantation of ^{19}F, ^{28}Si, ^{40}Ar, and ^{131}Xe into Si(100) at room temperature produces defects, which induce positive perpendicular strain. The strain is linearly proportional to the defect concentration with a universal coefficient of $B \sim 0.01$ over the whole damage range. Both defect concentration and strain rise nonlinearly with the dose for all ion species. In the low damage regime, the damage rises linearly with the dose. The slope of the damage versus the dose rises with increasing ion mass (from ^{19}F to ^{131}Xe), and is a quadratic function of the Frenkel pairs produced per unit dose of incident ions. We attribute the observed nonlinear behavior of damage produced by ion implantation at room temperature to the recombination of simple defects and their clustering to form stable defect complexes.

ACKNOWLEDGMENTS

This work was supported in part by the Semiconductor Research Corporation under contract No. 100-SJ-90, and by the National Science Foundation under grant No. DMR-8811795. The authors gratefully acknowledge this support.

[1] J. W. Mayer, L. Eriksson, S. T. Picraux, and J. A. Davis, Can. J. Phys. **46**, 663 (1968).
[2] D. J. Mazey, R. S. Nelson, and R. S. Barnes, Philos. Mag. **17**, 1145 (1968).
[3] F. F. Morehead, Jr. and B. L. Crowder, Radiat. Eff. **6**, 27 (1970).
[4] M. L. Swanson, J. R. Parsons, and C. W. Hoelke, *Radiation Effects in Semiconductors*, edited by J. W. Corbett and G. D. Watkins (Gordon and Breach, New York, 1971), p. 359.
[5] L. Chadderton and F. Eisen, Eds., *Proceedings of the 1st International Conference on Ion Implantation* (Gordon and Breach, New York, 1971).
[6] J. F. Gibbons, Proc. IEEE **60**, 1062 (1972).
[7] D. A. Thompson and R. S. Walker, Nucl. Instrum. Methods **132**, 281 (1976).
[8] J. R. Dennis and E. B. Hale, J. Appl. Phys. **49**, 1119 (1978).
[9] E. Glaser, G. Götz, N. Sobolev, and W. Wesch, Phys. Status Solidi A **69**, 603 (1982).
[10] M. O. Ruault, J. Chaumont, and H. Bernas, Nucl. Instrum. Methods **209/210**, 351 (1983).
[11] O. W. Holland, S. J. Pennycook, and G. L. Albert, Appl. Phys. Lett. **55**, 2503 (1989).
[12] J. Linnors and G. Holmen, Phys. Rev. B **32**, 2770 (1985).
[13] A. E. White, K. T. Short, R. C. Dynes, J. P. Garno, and J. M. Gibson, Appl. Phys. Lett. **50**, 95 (1987).
[14] P. A. Packan and J. D. Plummer, Appl. Phys. Lett. **56**, 1787 (1990).
[15] G. Bai and M-A. Nicolet, J. Appl. Phys. **70**, 649 (1991).
[16] J. P. Biersack and L. G. Haggmark, Nucl. Instrum. Methods **174**, 257 (1980).
[17] C. R. Wie, T. A. Tombrello, and T. Vreeland, Jr., J. Appl. Phys. **59**, 3743 (1986).
[18] J. W. Corbett, J. P. Karins, and T. Y. Tan, Nucl. Instrum. Methods **182/183**, 457 (1981).